

Scaling relations of the colour-detected cluster RzCS 052 at $z = 1.016$ and some other high-redshift clusters

S. Andreon,¹★ R. De Propris,² E. Puddu,³ L. Giordano^{1,4} and H. Quintana⁵

¹*INAF - Osservatorio Astronomico di Brera, via Brera 28, 20121, Milano, Italy*

²*Cerro Tololo Inter-American Observatory, La Serena, Chile*

³*INAF - Osservatorio Astronomico di Capodimonte, salita Moiarriello 16, 80131 Napoli, Italy*

⁴*Università degli Studi di Milano Bicocca, Piazza della Scienza 3, 20126 Milano, Italy*

⁵*Departamento de Astronomía y Astrofísica, Pontificia Universidad Católica de Chile, Santiago, Chile*

Accepted 2007 October 4. Received 2007 October 2; in original form 2007 May 23

ABSTRACT

We report on the discovery of the $z = 1.016$ cluster RzCS 052 using a modified red-sequence method, follow up spectroscopy and X-ray imaging. This cluster has a velocity dispersion of $710 \pm 150 \text{ km s}^{-1}$, a virial mass of $4.0 \times 10^{14} M_{\odot}$ (based on 21 spectroscopically confirmed members) and an X-ray luminosity of $(0.68 \pm 0.47) \times 10^{44} \text{ erg s}^{-1}$ in the [1–4] keV band. This optically selected cluster appears to be of richness class 3 and to follow the known $L_X\text{--}\sigma_v$ relation for high-redshift X-ray selected clusters. Using these data, we find that the halo occupation number for this cluster is only marginally consistent with what was expected assuming a self-similar evolution of cluster scaling relations, suggesting perhaps a break of them at $z \sim 1$. We also rule out a strong galaxy merging activity between $z = 1$ and today. Finally, we present a Bayesian approach to measuring cluster velocity dispersions and X-ray luminosities in the presence of a background: we critically reanalyse recent claims for X-ray underluminous clusters using these techniques and find that the clusters can be accommodated within the existing $L_X\text{--}\sigma_v$ relation.

Key words: methods: statistical – galaxies: clusters: general – galaxies: clusters: individual: RzCS 052 – galaxies: evolution – dark matter – X-rays: galaxies: clusters.

1 INTRODUCTION

Clusters of galaxies are not only a powerful tool to study galaxy evolution but can also be used to constrain cosmological parameters, resolving several parameter degeneracies (e.g. Allen et al. 2004; Albrecht et al. 2006). In particular, clusters at high redshifts ($z > 1$), of which only a handful are currently known, provide the greatest leverage in determining the nature of the acceleration constant (e.g. Rapetti et al. 2007). These determinations, however, rely on an accurate estimate of the cluster mass, whose uncertainty is arguably the dominant contributor to the error budget in deriving cosmological parameters from cluster statistics (Henry 2004; Albrecht et al. 2006).

Ideally, one wishes to apply the virial theorem to get a direct measurement of cluster masses. In fact, the dark matter velocity dispersion is an extremely good tracer of the halo masses in all simulations (Evrard et al. 2007), and galaxies are nearly unbiased velocity tracers (Evrard et al. 2007 and references therein; Rines, Diaferio & Natarajan 2007), in good agreement with previous works (Tormen, Bouchet & White 1997; Biviano et al. 2006). The mea-

surement of the cluster velocity dispersion requires a large number of radial velocities, which are observationally expensive to obtain, especially for high-redshift clusters. For this reason and because each mass estimator carries some key information, more commonly the scaling between pairs of more easily observable mass-related quantities is studied, such as X-ray luminosity, temperature or the Y_X (Kravtsov, Vikhlinin & Nagai 2006) parameter, or optical richness. These studies often look for outliers, however their search is blessed by data limitation: for example, in the search of clusters X-ray dim for their optical richness, Donahue et al. (2001) and Gilbank et al. (2004) both mostly worked with putative clusters (i.e. not spectroscopically confirmed) and X-ray undetections.

Only a few works directly address the relative quality of different mass estimators with velocity dispersion: Borgani & Guzzo (2001) compare the scatter of two mass estimators, X-ray luminosity and richness, and found that the former is a better mass tracer than the latter when the former is uniformly measured and the latter is taken from a 50 year old paper reporting eye estimate of the cluster optical richness (the Abell 1958 catalogue). In both CNOC (Canadian Network for Observational Cosmology) and nearby clusters, mass correlates better with richness than with X-ray luminosity (Yee & Ellingson 2003; Popesso et al. 2005). Eke et al. (2004) found that optical luminosity is a better proxy of mass than velocity dispersion

★E-mail: stefano.andreon@brera.inaf.it

in common conditions, i.e. when velocities are available for a small sample of galaxies. A related issue, which we will examine below, is whether there exist clusters that are X-ray dim for their mass (velocity dispersion) (e.g. Lubin, Mulchaey & Postman 2004; Johnson et al. 2006; Fang et al. 2007).

The relation between richness and mass has received some recent attention in the form of the halo occupation function (Berlind & Weinberg 2002; Lin, Mohr & Stanford 2004 and references therein) whose first moment is the halo occupation number (HON), the average number N of galaxies per cluster of mass M . In order to address the evolution of the HON, velocity dispersion information is often unavailable for a large cluster sample; mass and cluster size are inferred from other mass-related quantities (e.g. the X-ray temperature), and assumed to evolve self-similarly. The evolution of the HON with redshift is still unclear: the initial study by Lin et al. (2004) claimed that the HON increases at high redshift, but Lin et al. (2006) find evidence that it does not evolve strongly out to $z \sim 1$, suggesting that the galaxy population in clusters was established and assembled at early epochs. Muzzin et al. (2007) confirm the above, with a sample of reduced redshift leverage and hence reduced evolution sensitivity, but available velocity dispersion information.

Here, we present the photometric discovery, spectroscopic confirmation and X-ray properties of a new $z = 1.016$ cluster of galaxies (RzCS 052), a cluster optically rich but undetected in the *XMM*-Large Scale Structure (LSS) survey (Pierre et al. 2007), and hence possibly X-ray dark (i.e. dim for its mass). We derive its global properties (richness, X-ray luminosity, velocity dispersion and mass) and study these in the context of cluster scaling relations (L_X - σ , HON) at high redshift. In particular, we test the claim that the HON (the way galaxies populate cluster-scale haloes) has not changed $z \sim 1$ (Lin et al. 2006) under far less assumptions than the original claim. We also present a Bayesian approach to the determination of cluster velocity dispersion and X-ray luminosity and use it to critically examine recent claims about the existence of underluminous X-ray clusters. A companion paper (Andreon et al. 2007) addresses the use of RzCS 052 as a laboratory for studying galaxy formation and evolution.

We adopt $\Omega_\Lambda = 0.7$, $\Omega_m = 0.3$ and $H_0 = 70 \text{ km s}^{-1} \text{ Mpc}^{-1}$. Magnitudes are quoted in their native photometric system (Vega for R , SDSS for z').

2 THE DATA AND DATA REDUCTION

2.1 Photometry: CTIO Rz' images

Broadband images for a 7 deg^2 region around this cluster were obtained at the Cerro Tololo Inter-American Observatory (CTIO) Blanco 4-m telescope in the R and z' ($\lambda_c \sim 9000 \text{ \AA}$) filters using the Mosaic II camera. We use the same imaging data as Andreon et al. (2004a), where details on the data and their analysis are found. Briefly, Mosaic II is a 8192×8192 CCD camera with a 36 arcmin field of view at prime focus. Exposure times were 1200 s in R and 1500 s in z' : seeing was between 0.9 and 1.0 arcsec in the final images.

Source detection and photometry were carried out using SEXTRACTOR (Bertin & Arnouts 1996). Colours and magnitudes were computed within a fixed 2 arcsec (radius) aperture, and corrected for minor differences in seeing, as in Andreon et al. (2004a). Completeness magnitudes (5σ in a 3 arcsec aperture), computed as in Garilli, Maccagni & Andreon (1999), are $R = 24.0$ and $z' = 22.5$ mag.

Fig. 1 shows a true-colour image of RzCS 052, as derived from CTIO z' image and IRAC (Infrared Array Camera) *Spitzer* [3.6] and [4.5] images. *Spitzer* data reduction is described in Andreon (2006a), which also presents the composite stellar mass function and the $3.6 \mu\text{m}$ luminosity function (LF) of many clusters, including RzCS 052.

2.2 Spectroscopy

Multi-object spectroscopy was carried out on Gemini in late 2003, and on VLT in late 2003 and during 2004. On VLT, the spectra were taken using FORS2 (Focal Reducer and Low Dispersion Spectrograph 2) with the GRIS 300I and the OG590 filter for a total integration time of 11 ks. On Gemini, the spectra were obtained with the Gemini Multi-object Spectrograph (GMOS), operating in nod and shuffle mode (Cuillandre et al. 1994; Abraham et al. 2004) in order to perform accurate sky subtraction, with the R150 grating for a total integration time of 15 ks.

The GMOS package for IRAF was used to calculate the wavelength solutions and to reduce the multi-object observations into one-dimensional spectra. The RVSAO package (Kurtz & Mink 1998) was used to measure redshifts (and their errors) of target galaxies by cross-correlation with stellar and galaxy templates of known radial velocity (Tonry & Davis 1979).

A total of 57 spectra of 54 galaxies yielded reliable redshifts, with typical individual errors on redshift of 50 to 150 km s^{-1} (depending on instrument, exposure time, object spectrum, etc.). Three galaxies with duplicate observations have concordant redshifts in the two data sets. Fig. 2 shows the spectra of RzCS 052 members from the VLT run. Table 1 lists position and redshift of galaxies within 4000 km s^{-1} of RzCS 052.

2.3 XMM-EPIC data

RzCS 052 was observed with *XMM-Newton* using the European Photon Imaging Camera (EPIC) instrument (Jansen et al. 2001) in 2002 in full-frame mode with the thin filter. After flares filtering, the good exposure time is ~ 13 ks for the MOSes (Turner et al. 2001), and an ~ 8 ks for the PN (Strüder et al. 2001). By using the *XMM-Newton* Science Analysis System (SAS, v. 7) package and our own scripts, we kept only patterns between 0 and 12 for MOS and 0 to 4 for PN. We flagged bad pixels, bad columns and CCD gaps, regions not seen by all three instruments, as well as pixels contaminated by the flux of other sources. We remove the energy band [0.60–0.70] keV, where an instrumental line shows up because this flattens the sky background, and hence decreases the complexity of the model used to describe its spatial distribution. We merged the three instruments to improve signal-to-noise ratio (S/N).

For comparison, we also reduced EPIC observations of a cluster at almost identical redshift, XLSSC 029 at $z = 1.05$ (Andreon et al. 2005), just one degree apart from RzCS 052. To make the comparison straightforward, we cut the XLSSC 029 exposure to match (almost) exactly the exposure time of RzCS 052.

3 RESULTS

3.1 Photometric discovery and colour-magnitudes relation

RzCS 052 was initially detected in 2000 using photometric data (Rz') as a clustering of sources of similar colour using our own version (Andreon 2003; Andreon et al. 2004a,b) of the red-sequence method (Gladders & Yee 2000). This is shown in the right-hand panel of



Figure 1. True-colour (z' [3.6][4.5]) degraded-resolution (to make galaxies not too small when printed) image of a region of a 24 Mpc^2 area around RzCS 052. Spectroscopically confirmed clusters and isodensity contours for red galaxies are also marked. Note the number density contrast of reddish galaxies between the cluster centre and the right-hand part of the image. The ruler is 1 arcmin long; north is up and east is to the left-hand side.

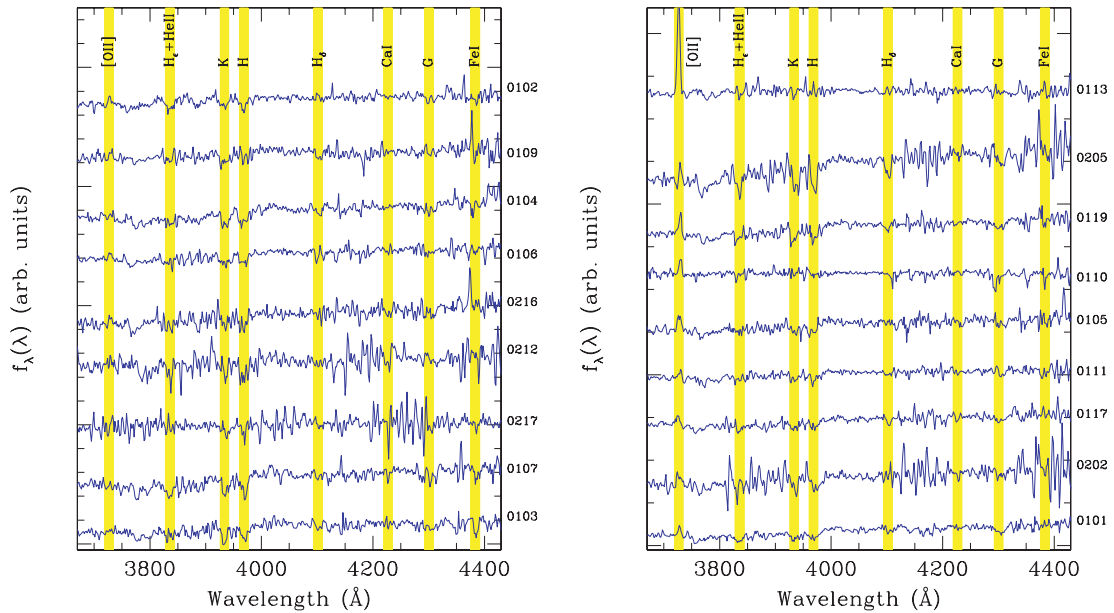


Figure 2. Spectra of RzCS 052 members coming the VLT run. We have vertically shifted the spectra and zoomed on a reduced wavelength range for display purpose.

Fig. 3, which shows that in a 2 arcmin circle centred on RzCS 052 (02:21:42 –03:21:47 J2000) there are 13 galaxies redder than $R - z' = 1.55 \text{ mag}$ (solid histogram), while the expected number in the same area (i.e. background, average number measured in a

0.36 deg^2 area all around the cluster) is ~ 2.1 , a very obvious over-density detection.

The colour of the red sequence (Fig. 3), compared to those of other high-redshift clusters presented in Andreon et al. (2004a), suggests a

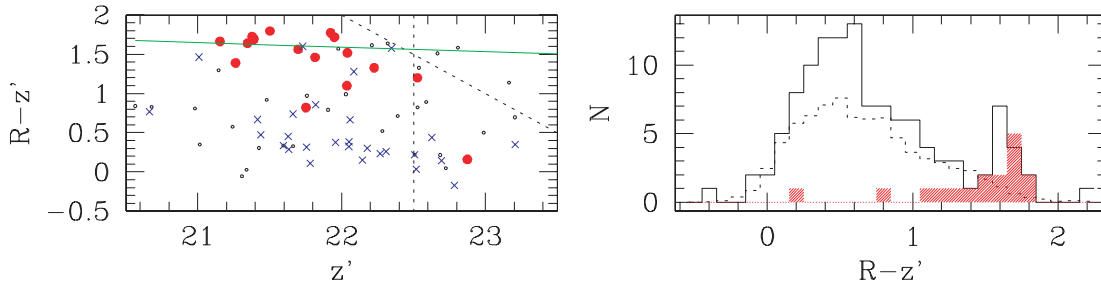


Figure 3. Left-hand side: colour–magnitude diagram for galaxies (close circles) within 1 arcmin from the cluster centre or with a known redshift (red closed circles for members, blue crosses for interlopers) using CTIO discovery data. R and z' mag completeness limits are show with dashed lines. The green line is the expected colour–magnitude at the cluster redshift, from Kodama & Arimoto (1997). Right-hand side: colour histograms of galaxies within 2 arcmin from the cluster centre (solid histogram), and of the average control field (measured on a 0.36 deg^2 area, dashed histogram), normalized to the cluster area. A clear excess is seen, especially at $R - z' > 1.5$ mag. The hashed histogram is the colour distribution of spectroscopically confirmed member galaxies. In both panels, a few objects with spectroscopic redshift are missing because they fall on bad CCD regions or have extreme colours.

Table 1. J2000 coordinates and redshift of galaxies within 4000 km s^{-1} (rest frame) of RzCS 052.

RA	Dec.	Redshift
02:21:36.21	−03:24:56.0	1.0210
02:21:37.08	−03:24:28.4	1.0192
02:21:37.60	−03:21:38.0	1.0176
02:21:38.85	−03:23:40.7	1.0206
02:21:39.60	−03:22:00.9	1.0217
02:21:40.32	−03:19:03.4	1.0225
02:21:40.46	−03:18:35.6	1.0158
02:21:41.13	−03:24:41.2	1.0195
02:21:41.73	−03:23:35.2	1.0089
02:21:42.04	−03:21:54.1	1.0132
02:21:42.14	−03:20:07.0	1.0074
02:21:42.52	−03:22:43.6	1.0156
02:21:42.81	−03:22:48.8	1.0181
02:21:43.15	−03:21:15.2	1.0065
02:21:43.87	−03:21:06.0	1.0129
02:21:43.96	−03:20:27.9	1.0159
02:21:44.85	−03:22:04.3	1.0230
02:21:44.90	−03:21:44.5	1.0145
02:21:45.21	−03:21:25.5	1.0187
02:21:45.24	−03:20:44.3	1.0151
02:21:48.33	−03:20:48.6	1.0160

redshift of $z \sim 1.0$. F. Barrientos (private communication) confirmed that this cluster has also been detected by their red-sequence cluster survey with which we share the CTIO imaging.

The right-hand panel of Fig. 3 shows that the colour distribution of RzCS 052 galaxies (the area between the solid and dashed histogram) is bimodal, displaying a narrow peak at $R - z' = 1.6$ mag and a broad excess at bluer colours. From now on, we define galaxies as red if $1.4 < R - z' < 1.9$ mag. Isodensity contours for red galaxies are shown in Fig. 1.

3.2 Spectroscopical confirmation and velocity dispersion

The upper panel of Fig. 4 shows the distribution of successfully measured redshifts in the cluster line of sight. The clear peak at $z \sim 1.02$ is in good agreement with the photometric redshift inferred from the colour of the red sequence ($z \sim 1.0$). The lower panel shows a detailed view around the cluster redshift. We measure $z_{\text{cluster}} = 1.016$ and $\sigma_v = 710 \pm 150 \text{ km s}^{-1}$ (see Appendix B for methods). The gapper or biweight estimators (Beers, Flynn & Gebhardt 1990) give identical σ_v .

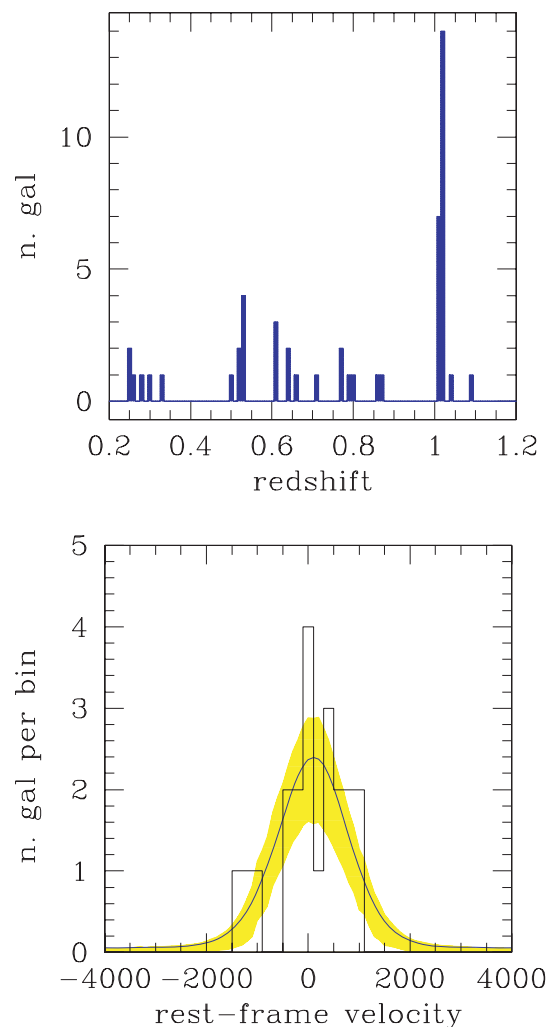


Figure 4. Redshift distribution of all successfully measured redshift in the cluster line of sight (top panel) and around the $z = 1.016$ (bottom panel). In the bottom panel, the curve marks the mean model, and the grey (yellow in colour) region is the 68 per cent highest density posterior interval.

3.3 Richness

Fig. 5 shows the spatial distribution of red galaxies (open points) in a wide area of 133 Mpc^2 around RzCS 052. Two galaxy overdensities are quite obvious, both colour detected by our cluster detection

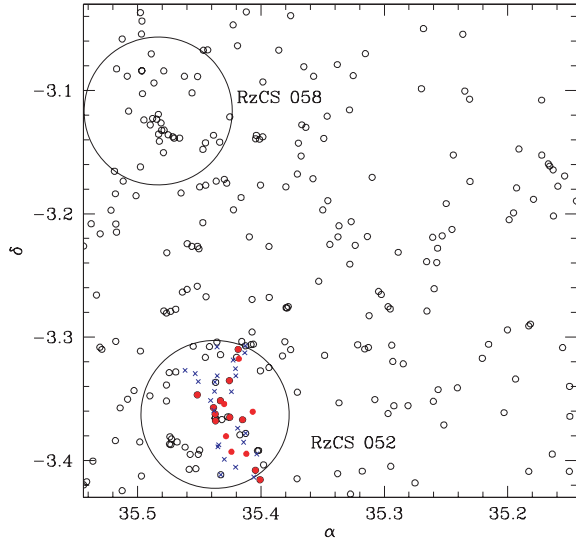


Figure 5. Spatial distribution of red galaxies (open points), spectroscopically confirmed members (solid red points) and spectroscopically confirmed interlopers (blue crosses).

algorithm. Spectroscopically confirmed RZCS 052 members (solid red points) and spectroscopically confirmed interlopers (crosses) are also marked. The two large circles have a radius of 3.6 arcmin, which is 80 per cent of the Abell (1958) radius (at the RZCS 052 redshift).

We fit a β profile to the distribution of galaxies (Appendix A) and remove contamination using counts from the field in Fig. 5, discarding the region around RZCS 058. Within one Abell radius, we find 56 ± 20 red cluster galaxies brighter than $z' = 22.5$ mag. This number must be corrected to $M_3 + 2$ using the luminosity function and the 30 per cent blue fraction measured in Andreon et al. (2007). The total number of galaxies is ~ 150 that qualifies RZCS 052 as an Abell richness class 3. A different richness estimate is presented in Section 4.

3.4 X-ray luminosity

The RZCS 052 cluster is within the *XMM*-LSS field, but not X-ray detected by the current *XMM*-LSS pipeline (Pierre et al. 2007),

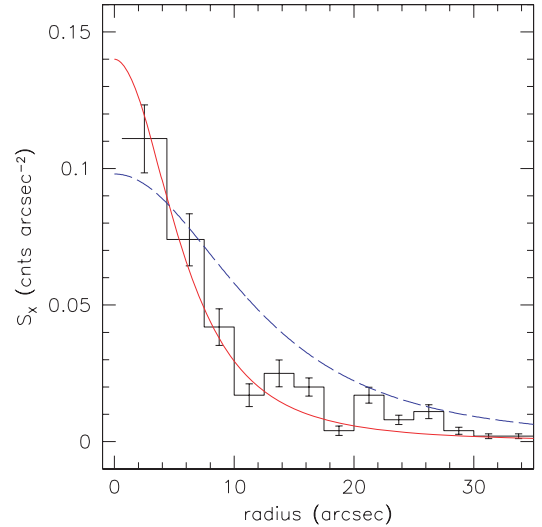


Figure 7. Radial profile of the foreground X-ray point source (black solid histogram) and of the *XMM* PN point spread function (red continuous line), at the off-axis angle of the source, and a $\beta = 2/3$ model having $r_c = 16$ arcsec (150 kpc if at the cluster distance, dashed blue line). The source is unresolved at the *XMM* resolution, the slight excess with respect to the PSF being due to the unremoved contribution of RZCS052, and far more compact than a β model with a typical cluster core radius at $z = 1$.

even though several other $z \sim 1$ clusters are (Valtchanov et al. 2004; Andreon et al. 2005; Bremer et al. 2006 and some more yet unpublished).

The left-hand panel of Fig. 6 shows the X-ray image of RZCS 052. The X-ray source close to the optical cluster centre is not extended (Fig. 7) and appears to coincide with a foreground spiral (as classified from *Hubble Space Telescope* images presented in Andreon et al. 2007) galaxy, and thus not associated with RZCS 052. Therefore, the flux from this source is discarded in the determination of the X-ray flux of RZCS 052.

The right-hand panel of Fig. 6 shows an X-ray image of a very similar (in redshift, off-axis angle and exposure time of observations) cluster: XLSSC 029. XLSSC 029 is much brighter than RZCS 052.

In order to determine the X-ray luminosities of XLSSC 029 and RZCS052, we use the method described in Appendix A. We

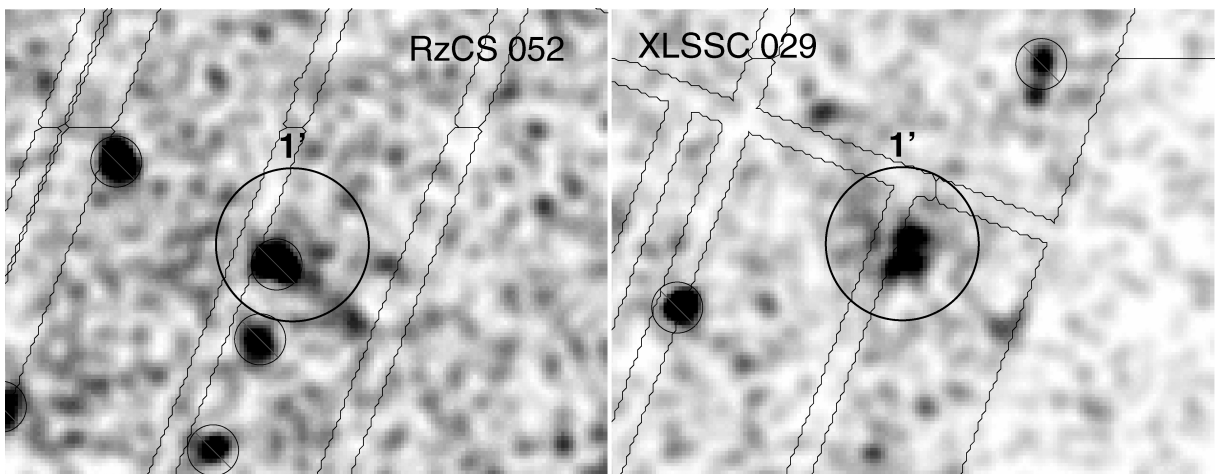


Figure 6. [0.5–2.0] keV image of RZCS 052 (left-hand panel) and XLSSC 029 (right-hand panel), at a very similar redshift and with matched X-ray images and smoothing. Pixels affected by other sources, or falling on CCD gaps, are marked by regions. Simple eye inspection confirms that RZCS 052 is much fainter than XLSS 029.

assume uniform priors, zeroed in the unphysical ranges (negative core radius, negative background intensity, negative central cluster intensity) and in ranges that make the total flux infinity (i.e. for $\beta < 0.4$). Besides returning a flux uncertainty that accounts for the covariance of all parameters, we also account for the cluster flux in the background region (for XLSSC 029, this turns out to lead to an underestimate of its count rate by 30 per cent).

For XLSSC 029, we found: $L_X[1-4]$ keV band: $4.4 \pm 0.8 \cdot 10^{44}$ erg s $^{-1}$, formally for a temperature of 4 keV (taken from Pierre et al. 2006), but actually for a range of temperatures because of our choice of quoting luminosities in the [1–4] keV band, i.e. in a band that, at the cluster redshift, matches the observer frame [0.5–2] band, and because of the very tiny dependency of the conversion factor on temperature. For RzCS 052, we found: $f_X = 1.2 \pm 0.8 \cdot 10^{-12}$ erg s $^{-1}$ cm $^{-2}$ and [1–4] keV rest-frame band $L_X = 0.68 \pm 0.47 \cdot 10^{44}$ erg s $^{-1}$ (both values are posterior mean and standard deviation). The cluster is not an ≈ 1.5 detection, however: the posterior probability $p(f_X < f_0 | data)$ goes to zero at fluxes $f_0 \gtrsim 1 \cdot 10^{-13}$ erg s $^{-1}$ cm $^{-2}$, i.e. the source has so many detected photons that data cannot be described by a model with a cluster signal fainter than f_0 , such as a model including background emissivity only. The large flux and intensity uncertainties account for the uncertainty of the beta function parameters (core radius, beta and central intensity) and background value.

3.5 L_X – σ_v relation

Fig. 8 shows the location in the L – σ_v plane of RzCS 052 cluster, with all the $z > 0.8$ clusters for which we found in the literature T , L_X and σ_v (Table 2). We ignored a few tentative σ_v determinations based on small number of velocities, because of being affected by large errors and by Eddington bias (detailed in Appendix B and in Section 3.6). Literature values of L_X are converted to the [1–4] keV band rest frame to minimize systematics.

RzCS 052 (closed circle) turns out to be one of the faintest and least massive (lower velocity dispersion) clusters known at $z > 0.8$. In spite of the cluster being optically selected, RzCS 052 has an X-ray luminosity appropriate for its mass (velocity dispersion), or at least, data are compatible with the trend seen for similar, but

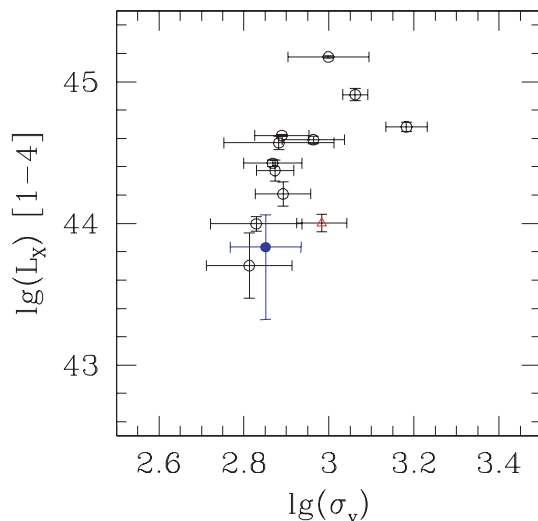


Figure 8. L_X – σ_v relation for literature clusters (open points) and for RzCS 052 (close point). The (red) triangle is CL1604+4304, i.e. the cluster originally claimed to be X-ray dark, at the revised value of the σ_v determination (see text for details).

X-ray selected, clusters. Therefore, although the X-ray luminosity of RzCS 052 is modest, it is consistent with measurements for other high-redshift clusters. This is reassuring for ongoing X-ray cluster surveys, which usually assume a Gaussian model for the scatter between mass and X-ray luminosity: RzCS 052 is not an example of a new class of clusters, massive but dark in X-ray, easily escaping the detection in X-ray surveys because of being faint for their mass. Instead, RzCS 052 has an X-ray luminosity appropriate for its mass (velocity dispersion) and it is missed in the *XMM*-LSS because of the low survey sensitivity at $z \sim 1$ for objects of RzCS 052 σ_v and obeying to the L_X – σ_v relation.

3.6 Are there known optically underluminous clusters or groups at high redshift?

With the Bayesian tools described in the Appendix, we revisit claims about the existence of underluminous X-ray clusters (i.e. clusters whose masses – from their velocity dispersions – are too large for their X-ray luminosity – which is often an upper limit). We have seen (Appendix B) that in the case of CL1604+4304 a Bayesian estimate of its velocity dispersion, as well as the revised value of $\hat{\sigma}_v$ published by Gal & Lubin (2004), makes this cluster no longer an outlier (i.e. underluminous) in the L_X – σ_v relation. We show here that Bayesian estimates of velocity dispersions and X-ray fluxes cast serious doubts on the existence of the X-ray underluminous groups or clusters claimed in literature.

Fang et al. (2007) studied seven DEEP2 (Deep Extragalactic Evolutionary Probe 2) groups at $0.75 < z < 1.03$. They derive an upper limit to the X-ray flux by considering only photons within an aperture of radius 30 arcsec, a metric radius of 250 kpc which is considered to be typical for groups and clusters at high redshift. However, assuming $\beta = 2/3$ (also a typical value), the X-ray flux outside of their aperture, integrated to infinity, is 2.4 times larger than the flux inside their aperture. The upper limit quoted by Fang et al. (2007) is therefore too small by a factor of 3.4.

Fang et al. (2007) derive their velocity dispersion from three to six galaxies. Because of Eddington (1940) biases, this is biased high: even symmetric errors move more low-velocity systems to high-velocity dispersion than otherwise. The Bayes theorem allows to correct for the bias, being the Eddington correction built in the Bayes theorem (Appendix B).

If these sources of error and biases are accounted for, the X-ray fluxes and velocity dispersions for the groups studied by Fang et al. (2007) are perfectly consistent with the local L_X – σ_v relation (Fig. 9). We note here that a similar argument can be made for the ‘underluminous’ CNOC groups claimed by Spiegel, Paerels & Scharf (2007), based on velocity dispersions computed on just three or four velocities, and upper limits on the X-ray luminosity.

Popesso et al. (2007) also claim that there exist X-ray underluminous clusters in the local Universe, but their definition of ‘underluminous’ depends on the data depth. Most of their underluminous clusters have normal X-ray luminosity for their mass, because they obey to the L_X – σ_v relation (see their fig. 2d), and are called ‘underluminous’ because they are faint in their X-ray imaging. Deeper data would have classified them as ‘normal’. The few remaining clusters are found to have a negative (unphysical) X-ray flux and seem underluminous in the L_X – σ_v relation because they are plotted at an arbitrary value of L_X rather than as an upper limit. Such objects are not underluminous in the generally understood sense.

To summarize, to our best knowledge there is no evidence for not even a single example of cluster (or group) of galaxies

Table 2. Luminosity and velocity dispersion of clusters at $z > 0.8$.

Name	z	$\log L_X[1-4]$	Ref.	σ_v	N	Ref.
RXJ1716+6708	0.813	44.68 ± 0.03	12	1522 ± 180	37	1
RXJ1821.6+6827	0.816	44.62 ± 0.01	2	775 ± 122	18	2
MS1054-30321	0.830	44.91 ± 0.04	12	1153 ± 80	..	3
RXJ0152-1357S	0.830	44.42 ± 0.02	12	737 ± 126	18	4
RXJ0152-1357N	0.835	44.59 ± 0.03	12	919 ± 168	16	4
RzCS 530	0.839	44.20 ± 0.09	5	780 ± 126	17	5
1WGA1226+3333	0.890	45.17 ± 0.01	12	997 ± 245	12	6
Cl1604+4304	0.900	44.00 ± 0.06	7,13	962 ± 141	67	7
RzCS 052	1.016	43.83 ± 0.37	This work	710 ± 150	21	This work
RXJ0910+5422	1.106	44.00 ± 0.05	12	675 ± 190	25	8
RXJ1252-2927	1.237	44.37 ± 0.07	12	747 ± 79	38	9
LynxW	1.270	43.70 ± 0.23	12	650 ± 170	9	10
1WGAJ2235.3	1.393	44.57 ± 0.05	11	762 ± 265	12	11

RzCS 530 is also known as XLSSC 003. References: 1: Gioia et al. (1999); 2: Gioia et al. (2004a); 3: Gioia et al. (2004b); 4: Demarco et al. (2005); 5: Valtchanov et al. (2004); 6: Maughan et al. (2004); 7: Gal & Lubin (2004); 8: Mei et al. (2006); 9: Demarco et al. (2007); 10: Stanford et al. (2001); 11: Mullis et al. (2005); 12: Ettori et al. (2004) and 13: Lubin et al. (2004).

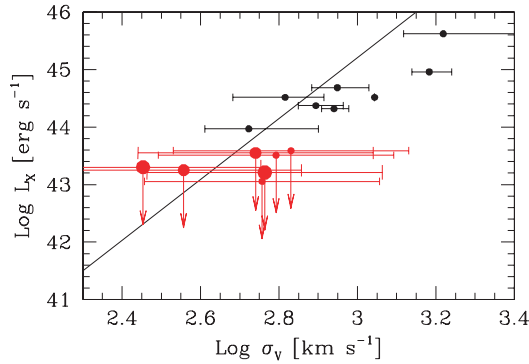


Figure 9. L_X - σ_v relation for literature clusters (close black points), as published by Fang et al. (2007), and DEEP2 groups and clusters, after our revision (red points and arrows). DEEP2 groups and clusters are no longer underluminous for their velocity dispersion.

X-ray dim for its velocity dispersion (once all sources of errors are accounted for), all previous claims proven to be based on uncertain grounds. If there are underluminous clusters, they have not yet been convincingly discovered.

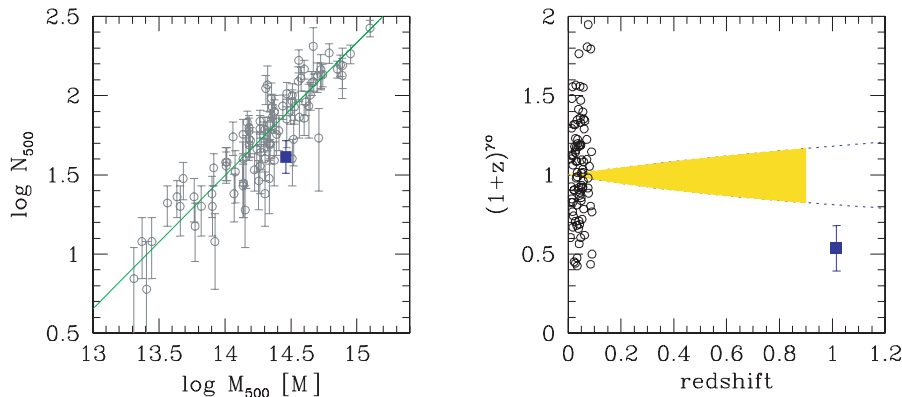


Figure 10. Left-hand panel: number of galaxies as a function of cluster mass. Open points mark local ($z < 0.1$) clusters and the filled (blue) square marks RzCS 052. The line is the Lin et al. (2006) fit to local clusters. Right-hand panel: evolution of the N - M relation. Symbols are as in left-hand panel. The shaded (yellow) region marks the 68 per cent confidence region derived by Lin et al. (2006) at $z < 0.9$.

4 HALO OCCUPATION NUMBER

We now derive the HON for RzCS 052. This basically requires an estimate of the N galaxies within a specified luminosity range and within a given cluster-centric radius and a mass estimate within the same spherical volume.

The virial radius, r_{200} , and mass, M_{200} , are derived from the virial theorem from the measured σ_v : $r_{200} = 1.04$ Mpc and $M_{200} = 4.0 \cdot 10^{14} M_\odot$. Adopting a Navarro, Frenk & White (1997) profile with concentration $c_{\text{dm}} = 5$, we derived $r_{500} = 0.69$ Mpc and cluster mass within r_{500} : $M_{500} = 2.9 \cdot 10^{14} M_\odot$.

The number of galaxies is computed by integrating the luminosity function within r_{500} down to $M^* + 3$. The latter is derived from the deeper VLT z' data presented in Andreon et al. (2007). Since the latter work count red galaxies only in their luminosity function, we correct for the blue galaxies fraction (adopting the blue fraction measured in Andreon et al. 2007). We also correct for the distribution of cluster members in a ‘cylinder’ outside the cluster sphere, assuming a NFW distribution with concentration $c_{\text{gal}} = 3$ (as in Lin et al. 2004, 2006). We opted for a Bayesian approach, because it simplify the computation of the uncertainty on the cluster richness fully accounting for uncertainties and covariances (neglected in past works) for all (Schechter and background) parameters. We

found $N_{500} = 41 \pm 11$ galaxies. Fig. 10 compares RzCS 052 to the local richness–mass scaling, showing that it is within the local relation, although near the bottom-end of the distribution.

Following Lin et al. (2006), we parametrize the evolution of $N(M, z)$ as

$$N(M, z) = N_0 (1+z)^\gamma (M/M_0)^s, \quad (1)$$

where $N_0 = 56$ and $M_0 = 2 \times 10^{14}$ are normalization factors of the relation, and $s = 0.84$ is the slope of the local relation derived by Lin et al. (2004) for their local cluster sample. We can rewrite this as below to emphasize the evolutionary terms:

$$(1+z)^{\gamma_0} = \frac{N_0(M, z)}{N_0 (M/M_0)^s}, \quad (2)$$

where we have added the subscript 0 to emphasize that we are now talking about the observed (or maximum-likelihood) values. In order to estimate γ , we can just look at the dependence of the RHS of equation (2) with $(1+z)$, as shown in the right-hand panel of Fig. 10. The value observed for RzCS 052 is a bit farther away in redshift than the range probed by Lin et al. (2006), and is outside their 68 per cent interval on γ , shown as shaded (yellow) area. A zero value would imply that the way galaxies populate cluster-scale haloes at $z = 0$ has not changed from $z = 1$. The size of the error bar on RzCS 052 is comparable to the error on γ (the width of shaded region in figure at $z = 1.0$), indicating that RzCS 052 alone carries comparable information to all the high-redshift clusters studied by Lin et al. (2006). Therefore, the data for RzCS 052 suggest a mild evolution, with the caveat that the scatter around the mean relation is large (see left-hand panel) and our result should be taken as tentative. We note, however, that our measurement is more direct than that of Lin et al. (2006): we include an estimate of the characteristic luminosity M^* and faint-end slope α from our data, whereas Lin et al. (2006) assumed them for the lack of data, and we measure mass and reference radius, r_{500} , from the virial theorem without assuming that they scale with X-ray temperature and evolve self-similarly, as assumed by Lin et al. (2006) for lack of direct measurements. The mild difference seen in the right-hand panel of Fig. 10 may indicate a possible break in the (assumed) self-similar evolution of the scaling between temperature and radius or mass at $z \sim 1$.

The parameter γ is the (logarithm) derivative of the redshift dependence of the number of galaxies per unit cluster mass, i.e. of the galaxy merging rate in appropriate units. Lin et al. (2006) and our results agree that the number of galaxies per unit cluster mass has increased (this work) or stayed constant (Lin et al. 2006) since $z = 1$. Therefore, both studies directly show that no intense merging activity of galaxies has been ongoing in clusters in the last 7 Gyr.

5 SUMMARY

We have identified a distant cluster from a modified red-sequence method and followed it up spectroscopically. RzCS 052 is a richness class 3 cluster at $z = 1.016$ with a velocity dispersion of $710 \pm 150 \text{ km s}^{-1}$ and an X-ray luminosity of $0.68 \pm 0.47 \times 10^{44} \text{ erg s}^{-1}$.

In spite of its optical detection, RzCS 052 obeys to the high-redshift $L_X\text{--}\sigma_v$ relationship as other X-ray selected clusters to the high-redshift $L_X\text{--}\sigma_v$ relationship, whereas in principle variations in the dynamical state of the clusters or in the thermal history of the intracluster medium may have moved it away from the $L_X\text{--}\sigma_v$ relation.

Analysis of the $N\text{--}M$ scaling shows that RzCS 052 has the right number of galaxies (actually, a bit less) than it should have for its mass, ruling out intense merging (among galaxies) activities in clusters from $z = 1$ to today, in agreement with Lin et al. (2006).

We present a Bayesian approach to measuring cluster velocity dispersions (most useful for sparsely sampled data and in the presence of a background) and X-ray luminosities or upper limits (essential in the case of poorly determined parameters). Critical re-analysis of the data of clusters/groups claimed to be outliers of the $L_X\text{--}\sigma_v$ relationship leads to conclude that there are no known, thus far, examples of clusters X-ray underluminous for their velocity dispersion. The above result is quite reassuring for the ongoing X-ray surveys: there is thus far no example of cluster missed because of an anomalous L_X for the cluster mass.

ACKNOWLEDGMENTS

We thank the referee for useful comments that improved the paper presentation. SA thanks A. Diaferio, Ben Maughan, A. Muzzin for useful discussions. This paper is based on observations obtained, with CTIO (prog. 2000-0295), European southern observatory (ESO; 072.C-0689, 072.A-0249, 073.A-0564, 074.A-0360), Gemini (GS-2003B-Q-18) *XMM* (Obs. ID. 0037980601). We acknowledge partial financial support from contract ASI-INAF I/023/05/0 and Centro de Astrofísica FONDAP.

REFERENCES

- Abell G. O., 1958, *ApJS*, 3, 211
 Abraham R. G. et al., 2004, *AJ*, 127, 2455
 Albrecht A. et al., 2006, preprint (astro-ph/0609591)
 Allen S. W., Schmidt R. W., Ebeling H., Fabian A. C., van Speybroeck L., 2004, *MNRAS*, 353, 457
 Andreon S., 2003, *A&A*, 409, 37
 Andreon S., 2006a, *A&A*, 448, 447
 Andreon S., 2006b, *MNRAS*, 369, 969
 Andreon S., 2008, *Bayesian Methods in Cosmology*. Cambridge University Press, Cambridge
 Andreon S., Punzi G., Grado A., 2005, *MNRAS*, 360, 727
 Andreon S., Willis J., Quintana H., Valtchanov I., Pierre M., Pacaud F., 2004a, *MNRAS*, 353, 353
 Andreon S., Willis J., Quintana H., Valtchanov I., Pierre M., Pacaud F., 2004b, *XXXIX Rencontres de Moriond, Exploring the Universe*. (astro-ph/0405574)
 Andreon S., Valtchanov I., Jones L. R., Altieri B., Bremer M., Willis J., Pierre M., Quintana H., 2005, *MNRAS*, 359, 1250
 Andreon S., Quintana H., Tajer M., Galaz G., Surdej J., 2006, *MNRAS*, 365, 915
 Andreon S., Puddu E., de Propris R., Cuillandre J.-C. 2007, *MNRAS*, submitted
 Beers T. C., Flynn K., Gebhardt K., 1990, *AJ*, 100, 32
 Berlind A. A., Weinberg D. H., 2002, *ApJ*, 575, 587
 Bertin E., Arnouts S., 1996, *A&AS*, 117, 393
 Biviano A., Murante G., Borgani S., Diaferio A., Dolag K., Girardi M., 2006, *A&A*, 456, 23
 Borgani S., Guzzo L., 2001, *Nat*, 409, 39
 Bremer M. N. et al., 2006, *MNRAS*, 371, 1427
 Cuillandre J. C. et al., 1994, *A&A*, 281, 603
 Demarco R. et al., 2005, *A&A*, 432, 381
 Demarco R. et al., 2007, *ApJ*, 663, 164
 Donahue M. et al., 2001, *ApJ*, 552, L93
 Eddington A. S., 1940, *MNRAS*, 100, 354
 Ettori S. et al., 2004, *MNRAS*, 354, 111
 Eke V. R. et al., 2004, *MNRAS*, 355, 769
 Evrard A. E. et al., 2007, *ApJ*, in press (astro-ph/0702241)
 Fang T. et al., 2007, *ApJ*, 660, L27
 Gal R. R., Lubin L. M., 2004, *ApJ*, 607, L1
 Garilli B., Maccagni D., Andreon S., 1999, *A&A*, 342, 408

- Gilbank D. G., Bower R. G., Castander F. J., Ziegler B. L., 2004, MNRAS, 348, 551
- Gioia I. M., Henry J. P., Mullis C. R., Ebeling H., Wolter A., 1999, AJ, 117, 2608
- Gioia I. M., Wolter A., Mullis C. R., Henry J. P., Böhringer H., Briel U. G., 2004a, A&A, 428, 867
- Gioia I. M., Braito V., Branchesi M., Della Ceca R., Maccacaro T., Tran K.-V., 2004b, A&A, 419, 517
- Gladders M. D., Yee H. K. C., 2000, AJ, 120, 2148
- Henry J. P., 2004, ApJ, 609, 603
- Jansen F. et al., 2001, A&A, 365, L1
- Jeffreys H., 1938, MNRAS, 98, 190
- Johnson O. et al., 2006, MNRAS, 371, 1777
- King I., 1962, AJ, 67, 471
- Kravtsov A. V., Vikhlinin A., Nagai D., 2006, ApJ, 650, 128
- Kodama T., Arimoto N., 1997, A&A, 320, 41
- Kurtz M. J., Mink D. J., 1998, PASP, 110, 934
- Lin Y.-T., Mohr J. J., Stanford S. A., 2004, ApJ, 610, 745
- Lin Y.-T., Mohr J. J., Gonzalez A. H., Stanford S. A., 2006, ApJ, 650, L99
- Lubin L. M., Mulchaey J. S., Postman M., 2004, ApJ, 601, L9
- Maughan B. J., Jones L. R., Ebeling H., Scharf C., 2004, MNRAS, 351, 1193
- Mei S. et al., 2006, ApJ, 639, 8
- Metropolis N., Rosenbluth A., Rosenbluth M., Teller A., Teller E., 1953, J. Chem. Phys., 21, 1087
- Mullis C. R., Rosati P., Lamer G., Böhringer H., Schwöpe A., Schuecker P., Fassbender R., 2005, ApJ, 623, L85
- Muzzin A., Yee H. K. C., Hall P. B., Lin H., 2007, ApJ, 663, 150
- Navarro J. F., Frenk C. S., White S. D. M., 1997, ApJ, 490, 493
- Pierre M. et al., 2006, MNRAS, 372, 591
- Pierre M. et al., 2007, MNRAS, in press
- Plionis M., Basilakos S., Georgantopoulos I., Georgakakis A., 2005, ApJ, 622, L17
- Popesso P., Biviano A., Böhringer H., Romaniello M., Voges W., 2005, A&A, 433, 431
- Popesso P., Biviano A., Böhringer H., Romaniello M., 2007, A&AB, 461, 397
- Postman M., Lubin L. M., Oke J. B., 2001, AJ, 122, 1125
- Rapetti D., Allen S. W., Amin M. A., Blandford R. D., 2007, MNRAS, 375, 1510
- Rines K., Diaferio A., Natarajan P., 2007, ApJ, 657, 183
- Spiegel D. S., Paerels F., Scharf C. A., 2007, ApJ, 658, 288
- Stanford S. A., Holden B., Rosati P., Tozzi P., Borgani S., Eisenhardt P. R., Spinrad H., 2001, ApJ, 552, 504
- Strüder L. et al., 2001, A&A, 365, L18
- Turner M. J. L. et al., 2001, A&A, 365, L27
- Tony J., Davis M., 1979, AJ, 84, 1511
- Tormen G., Bouchet F. R., White S. D. M., 1997, MNRAS, 286, 865
- Valtchanov I. et al., 2004, A&A, 423, 75
- Yee H. K. C., Ellingson E., 2003, ApJ, 585, 215

APPENDIX A: MIXTURE MODELLING OF INHOMOGENEOUS PROCESSES FOR THE L_X AND RICHNESS ESTIMATES

We want to measure a structured (i.e. not constant in space) Poisson signal in the presence of a background. We assume that the background (photons, galaxies, etc.) distribution is a homogeneous (i.e. the intensity is independent of position) Poissonian random process, whereas the cluster contribution is an inhomogeneous Poissonian random process whose intensity is given by an $I(r)$ radial profile. Provided that quantities are Poisson distributed, it does not matter if we are talking about galaxies (as in Section 3.3), or X-ray photons (as in Section 3.4), or something else.

Let us call θ the (unknown) set of parameters of the function $I(r)$. Simple algebra shows that the likelihood function $\mathcal{L}(\theta) \equiv p(r_i|I(r))$

is

$$\mathcal{L}(\theta) = \prod_i \omega(r_i) I(r_i) e^{-\int_{\Omega} \omega(r) I(r)}, \quad (\text{A1})$$

where Ω is the solid angle. The expression can be simplified somewhat by noting that the infinitesimal solid angle at r_i , $\omega(r_i)$, is independent of the parameter θ and therefore can be dropped. There are no limitations on the complexity of the shape of the solid angle. Ω also encodes the relative efficiency of the different parts of the instruments (e.g., the different efficiency of off- and on-axis response).

Combined with prior probability distributions for the parameters, this likelihood function yields, via the Bayes theorem, the posterior distribution for the function parameters θ , given the data. Markov Chains Monte Carlo (Metropolis et al. 1953) with a Metropolis et al. (1953) sampler is used to sample the posterior. The chain provides a sampling of the posterior that directly gives credible intervals for whatever quantity, either for the parameters θ or for any derived quantity such as total richness (or flux): for an interval at the desired credible level it is simply a matter of taking the interval that includes the relevant percentage of the samplings. Credible intervals (yellow area in Fig. 4 and B1) are computed in that way. Upper limits may be determined in the same way as fluxes for detection, i.e. by specifying the credible interval we are interested in.

The function $I(r)$ can be whatever function positively defined and having a finite integral. In this paper, we use a modified β function:

$$I(r) \propto [(1 + r/r_c)^2]^{-3\beta+1/2} + bkg, \quad (\text{A2})$$

where we have accounted for a constant background, bkg . By choosing a more complex background function, as in Andreon (2006b), we obtain the aimed mixture modelling of two inhomogeneous Poissonian processes.

A1 Fallacies of the usual measurements of L_X upper limits

While our way of determining fluxes, richness and their errors, as well as L_X upper limits, is unusual in our astronomical context (but the standard approach in other fields of astronomy and in statistics), we were obliged to introduce it because previous approaches are unsatisfactory when an important parameter has a large error or is undetermined.

A common assumption of many determinations of upper limits to the X-ray flux from a cluster is that the object flux is fully inside a given aperture or the object core radius and β are known. However, this is a dangerous assumption: if the object is undetected, its extent, core radius and β are not constrained. If, for example, the object is much larger than assumed or β is small (and data tell nothing about that, being the object undetected) the assumption has important consequences. For example, it is sufficient to assume that the ‘underluminous’ groups of Fang et al. (2007) have ‘typical’ core radii to make their L_X compatible with the local $L_X-\sigma_v$ relation (and the groups no longer underluminous).

A first step in the right direction is to correct for the flux outside the aperture, but this assume to know the unknown: when r_c and β are unmeasured, or are very poorly determined, we cannot assume them as perfectly known and we cannot make inferences dealing with quantities strongly depending on the poorly determined parameters, such as the location of clusters in the $L_X-\sigma_v$ relation. The scientific method does not suggest to *hope* to have taken, by good chance, the correct value of an unknown parameter (as r_c) when it strongly affects the result.

However, this is exactly the kind of problem where Bayesian approaches are most valuable. Bayes’ theorem allows us to infer

the value of a quantity (in this case L_X) in the presence of a nuisance parameter (core radius or β) whose value is unknown but whose value affects the measurement of the quantity. Assuming a single value for nuisance parameters artificially collapses the error ellipse along one (or more) axes and leads to an incorrectly small error bar and to call outlier something that instead is fully compatible with the model. The sum rule of probability prescribes to marginalize (average over) nuisance parameters, not to keep them fixed.

Other authors determine upper limit to the X-ray flux mistakenly taking the maximum-likelihood estimate of sampling theories, *total – background*, for the true value of the net flux. While *total – background* is allowed to be negative, the true value of the net flux cannot be. These two quantities differ when the net flux is comparable to background fluctuations (e.g. appendix B of Andreon et al. 2006).

Another common way to compute the upper limit of the X-ray flux is by measuring the fluctuations of background counts. While this number is interesting in its own right and has the appealing property that it becomes smaller and smaller with lower and lower background fluctuations, it is measuring something different than the X-ray flux. In fact, this quantity is a p -value, i.e. a measure of how frequently one observes larger background fluctuations under the null hypothesis that no (cluster) signal is there, which differs from how probable a signal can be there without detecting it. A pedagogical astronomer-oriented explication of the difference of the two concepts is presented in Andreon (2008).

APPENDIX B: MIXTURE MODELLING FOR σ_v MEASUREMENTS

We want to measure the scale (dispersion) of a distribution (say, of velocities), knowing that the sample is contaminated by the presence of interlopers, but without the knowledge of which object is an interloper. The main idea is not to identify or de-weight interlopers in the scale estimate, but to account for them statistically, precisely as astronomers do with photons when estimating the flux of a source in the presence of a background. The small size of astronomer samples (e.g. of cluster galaxies with known velocity) makes the asymptotic properties of frequentist estimators never reached in real life experiments and oblige us to look for a solution in the Bayesian paradigm.

Here, we assume that data come from two populations: background galaxies, whose distribution is assumed to be a homogeneous (i.e. the intensity is independent on v) Poissonian random process, and cluster galaxies, whose distribution is assumed to be a Poissonian process whose intensity is given by a Gaussian. The likelihood is given by equation (A1), with changes of variable names: Ω continues to be Ω , but it is easier to understand it if we call it Δv , the (velocity) range over which velocities are considered (say, $\pm 5000 \text{ km s}^{-1}$ from the cluster preliminary velocity centre). Ω is more appropriate than Δv as it accounts for intervals of complicated shape; r in Appendix A is now v and $I(v)$ is given by the sum of a Gaussian and a constant, with unknown weights, N_{clus} and N_{bkg} (respectively). Finally, each measured velocity v has an uncertainty σ_v . Therefore, $I(v)$ reads as

$$I(v) = \frac{N_{\text{clus}}}{2\pi\sqrt{\sigma_v^2 + \sigma_{\text{clus}}^2}} e^{-\frac{(v-v_{\text{clus}})^2}{2(\sigma_v^2 + \sigma_{\text{clus}}^2)}} + \frac{N_{\text{bkg}}}{\Delta v}. \quad (\text{B1})$$

Most literature estimates of cluster velocity dispersions are based on the family of estimators presented by Beers, Flynn & Gebhardt (1990). However, in the presence of a background and interlopers, with sparsely sampled data, a Bayesian estimator may be more appropriate.

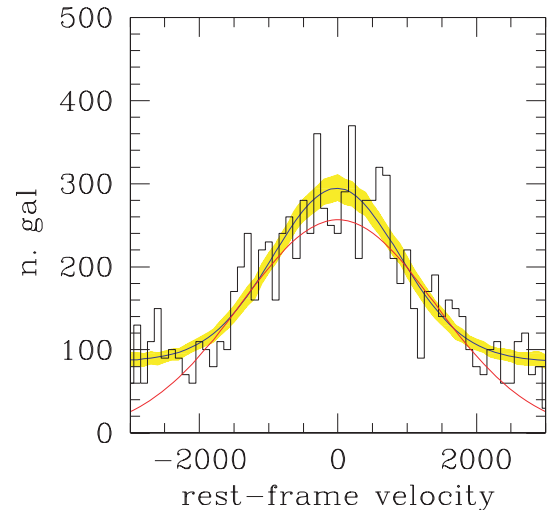


Figure B1. Velocity histogram for a simulated data set composed of 500 member galaxies drawn from a Gaussian having true $\sigma_v = 1000 \text{ km s}^{-1}$ and 500 interlopers drawn from a uniform distribution. The red curve is the cluster velocity estimate derived from robust statistics (0), whereas the blue curve and the shaded yellow region show the Bayesian estimate: $\sigma_v = 940 \pm 85 \text{ km s}^{-1}$ (see text for details).

A ‘real life’ example may suffice. The cluster C11604+4304 was regarded as unusually X-ray dim for the large mass estimated from a sample of 27 redshifts $\hat{\sigma}_v = 1226_{-154}^{+245} \text{ km s}^{-1}$ (Postman, Lubin & Oke 2001). However, the Bayesian method returns $\sigma_v = 1022 \pm 570 \text{ km s}^{-1}$ (posterior mean and standard deviation), which no longer makes the cluster X-ray underluminous and has a more realistic error bar. A larger sample of redshifts for this cluster, from Gal & Lubin (2004), revises the original estimate to $\hat{\sigma}_v = 962 \pm 141 \text{ km s}^{-1}$, in good agreement with the Bayesian estimate. With this value, the cluster is no longer X-ray underluminous.

Let us now consider a simulated ‘cluster’ composed of 500 galaxies distributed in a Gaussian with $\sigma_v = 1000 \text{ km s}^{-1}$ and superposed over a background of 500 uniformly distributed (in velocity) interlopers. The large sample size has been adopted to leave data to speak by themselves. Applying the methods of Beers et al. (1990) yields $\hat{\sigma}_v = 1400 \text{ km s}^{-1}$ which is an excessively large estimate of σ_v (and hence of mass), as also visible in Fig. B1 by simple inspection (compare the red curve and the histogram). The Bayesian posterior mean is $\sigma_v = 940 \pm 85 \text{ km s}^{-1}$ which is closer to the ‘true’ value (blue curve with shading). This simulation shows that the amplitude of bias of the Beers et al. estimator is systematic (i.e. it is present even for a large sample), and it is actually independent on the sample size, provided the relative fraction of cluster and interlopers is kept, although harder and harder to note as the sample size decreases because the estimator variance increases and dominates the scatter.

We now assess the sensitivity to model assumptions. Let us suppose that cluster substructure perturbs the velocity distribution, that we now assume to be described by

$$p(v) \propto e^{v/1000} (1 + e^{2.75v/1000})^{-1} \quad (\text{B2})$$

depicted in Fig. B2 (solid line). The function has first and second moments (mean and dispersion) equal to -460 and 1130 km s^{-1} , respectively. We simulate 1000 (virtual) clusters of 25 members each (and no interlopers) drawn from the distribution above (equation B2), but we compute the velocity dispersion using equation (B1), i.e. with a likelihood function appropriate for members

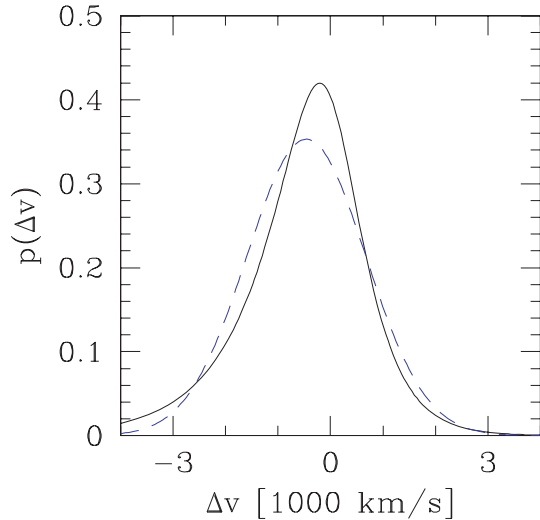


Figure B2. Perturbed velocity distribution (solid line), given by equation (B2), and a Gaussian with identical first two moments (dashed blue line). The former is used to generate hypothetic data and the latter is assumed to estimate σ_v .

drawn from a Gaussian. The mean of found posterior means is $\sigma_v = 1140 \text{ km s}^{-1}$ (versus the 1130 km s^{-1} input value) with a standard deviation of 185 km s^{-1} . The mean error uncertainty (posterior standard deviation) is 163 km s^{-1} , close (as it should be) to the scatter of the posterior means. The uncertainty has a negligible scatter, 18 km s^{-1} , indicating the low noise level of each individual uncertainty determination, four time lower than the scatter of the uncertainty of the biweight estimator of scale (70 km s^{-1}), that instead shows values as small as 73 km s^{-1} and as large as 865 km s^{-1} for data that are supposed to give a unique, fixed, value of uncertainty.

As a more difficult situation, we now consider a sample drawn, as before, from a distribution different from the one used for the analysis, but furthermore ~ 50 per cent contaminated by interlopers and consisting of half as many members: 13 galaxies are drawn from the distribution above (equation B2), superposed to a background of 12 galaxies, uniformly drawn from $\pm 5000 \text{ km s}^{-1}$. The mean of found posterior means is $\sigma_v = 1160 \text{ km s}^{-1}$ (versus the 1130 km s^{-1} input value). The mean error uncertainty is 390 km s^{-1} , with a low (80 km s^{-1}) scatter. The biweight estimator returns, on average, a strongly biased estimate $\hat{\sigma}_v = 2135 \text{ km s}^{-1}$.

The Bayesian determination of the cluster velocity dispersion already embodies the correction for the Eddington bias: the prior (i.e. the number distribution of objects having σ_v) does matter when the likelihood is shallow (i.e. when the data do not tightly constraint the aimed quantity), because, as well known to astronomers, if there are many more low-velocity systems than high-velocity dispersion systems the observed value (i.e. the maximum-likelihood value) is a biased estimate of the ‘true’ value. As point out by Jeffreys (1938), the Bayes theorem quantifies the bias, and we used it for computing the correction to Fang et al. (2007) velocity dispersions. Specifically, we assume a logarithmic slope of -0.6 for the prior and we follow appendix A of Andreon et al. (2006), because Fang et al. (2007) do not publish individual velocities for their systems.

Beers, Flynn & Gebhardt (1991) scale estimators work correctly in many cases, as shown in their paper. In these cases, the Bayesian approach returns similar numbers. We have shown, however, that in frontier-line cases, i.e. in the presence of an important background, or with sparsely sampled data, the Bayesian method returns better behaved quantities, less biased and less noisy.

This paper has been typeset from a $\text{\TeX}/\text{\LaTeX}$ file prepared by the author.